Chemical Engineering Journal 166 (2011) 715–725

Contents lists available at ScienceDirect

Chemical Engineering Journal

journal homepage: www.elsevier.com/locate/cej

Turbulently flowing liquid–liquid dispersions. Part I: Drop breakage and coalescence

F. Azizi*, A.M. Al Taweel

Multiphase Mixing and Separation Research Lab, Department of Process Engineering and Applied Sciences, Dalhousie University, Halifax, NS B3J 2X4, Canada

ARTICLE INFO

Article history:
Received 8 September 2010
Received in revised form
11 November 2010
Accepted 12 November 2010

Keywords:
Breakage
Coalescence
Liquid–liquid dispersion
Drop size distribution
Population balance
Static mixers

ABSTRACT

A successful attempt to simulate turbulently flowing liquid–liquid dispersions was undertaken in this work where the turbulent dispersion/coalescence of drops was accurately predicted over a wide range of operating conditions using the model developed by Coulaloglou and Tavlarides (1977) [36]. Experimental data obtained from an intensified liquid–liquid reactor/contactor in which screen-type static mixers were used to superimpose an adjustable uniformly distributed turbulence field on the nearly plug flow conditions encountered in high velocity pipe flows were used to validate the model predictions.

Drop size distribution and the Sauter mean diameter (when quasi-steady state conditions were assumed to be reached) were compared with the experimental results measured by photographic techniques and good agreement was obtained at different flow velocities and diverse screen geometries.

The use of mutli-stage screen-type static mixers where alternating breakage-dominated and coalescence dominated regions exist allowed the development of accurate model parameters that may be used for simulating other more complex liquid–liquid contacting conditions such as those encountered in mechanically agitated tanks.

1. Introduction

Despite the extensive literature dealing with both the hydrodynamic and interface science aspects, the dispersion of immiscible liquids remains one of the most difficult and least understood mixing problems, where minor changes in the chemical composition of the system would drastically affect its performance [1]. Consequently, the majority of the liquid–liquid contactors/reactors presently used are inefficiently designed with subsequent adverse effects on the reaction yield and selectivity and/or the mass transfer performance.

Stirred vessels, rotor–stator mixers, static mixers, valve or jet homogenizers, and extraction columns, are examples of industrial process equipments used to contact liquid–liquid systems. Due to the very complex hydrodynamic conditions prevalent in most of these commercially available contactors/reactors, designing such units is very difficult without an extensive employment of empiricism. However, the widespread use of empirical correlations poses several limitations as they conceal many of the hydrodynamic details and non-idealities [2]. Consequently, such results cannot be used over parameter ranges not included in the original measurement data set without the incorporation of excessive safety margins, thus requiring an extensive amount of pilot-scale testing. Therefore, a detailed understanding of the mixing process combined with the ability to accurately predict the volumetric mass transfer coefficient in such units can help in optimizing the performance, economy, and safety of these industrial systems.

Stirred tank reactors/contactors are the most commonly used in the chemical process industries, however, the operating conditions; the agitator and vessel geometry, as well as the positions of the inlet and outlet streams have direct impact on the tank's performance as they determine the hydrodynamics and turbulence intensities in the vessel. Nevertheless, these types of reactors suffer from many drawbacks as they lack uniformity, where mixing, drop size distributions, hold-up, and temperature profiles have large local variations [3].

On the contrary, plug flow reactors serve as a better choice in order to understand the complex phenomena taking place as well as providing better performance and control over the mixing, breakage and coalescence of drops, as well as heat and mass transfer. Moreover, tubular reactors equipped with static mixers have been gaining strong momentum in the chemical industries as they present an attractive alternative to conventional agitation since similar and sometimes better performance can be achieved at lower cost [4]. A common feature of these reactors is that turbulence is continuously produced and dissipated along the reactor. The turbulence is more homogeneous and nearly isotropic compared to a stirred tank reactor where most turbulence is pro-

* Corresponding author. Present address: Chemical Engineering Program, American University of Beirut, P.O. Box 11-0236, Riad El Solh, Beirut 1107 2020, Lebanon. Tel.: +961 1 374374x3439; fax: +961 1 744462.
E-mail address: fouad.azizi@aub.edu.lb (F. Azizi).

1385-8947/$ – see front matter © 2010 Elsevier B.V. All rights reserved.
doi:10.1016/j.cej.2010.11.050

Nomenclature

a	interfacial area of contact between the phases [m^{-1}]
b	wire diameter [m]
B_b	rate of particle generation by breakage per unit volume [$m^{-3}\,s^{-1}$]
B_c	rate of particle generation by coalescence per unit volume [$m^{-3}\,s^{-1}$]
C	turbulence decay equation constant [−]
$C_{1,\ldots,3}$	empirical constants [−]
C_4	empirical constant [m^{-2}]
d	drop diameter [m]
$d_{32,exp}$	experimentally measured Sauter mean diameter [m]
$d_{32,sim}$	simulated Sauter mean diameter [m]
D_b	rate of particle destruction by breakage per unit volume [$m^{-3}\,s^{-1}$]
D_c	rate of particle destruction by coalescence per unit volume of a parent particle [$m^{-3}\,s^{-1}$]
$g(d')$	breakage frequency of drops of diameter d' [s^{-1}]
$h(d,d')$	coalescence intensity of drops of diameter d and d' [s^{-1}]
L	distance between 2 consecutive screens [mm]
L_M	total mixer length [m]
M	screen mesh size [m]
n	turbulence decay equation exponent [−]
$N(d,t)$	number density function [m^{-3}]
u'	root mean square velocity fluctuation [$m\,s^{-1}$]
U	mean velocity [$m\,s^{-1}$]
v	droplet volume [m^3]
x	distance down the screen [m]
x_o	virtual origin of turbulence decay [m]

Greek letters

α	fraction open area of the screen [−]
$\beta(d,d')$	probability that a drop of size d' is formed when a drop d breaks [−]
ΔP	pressure drop [$N\,m^{-2}$]
ε	energy dissipation rate [$m^2\,s^{-3}$]
$\lambda(d,d')$	coalescence efficiency [−]
σ	interfacial tension [$N\,m^{-1}$]
μ	viscosity [$kg\,m^{-1}\,s^{-1}$]
$\nu(d)$	number of daughter drops formed by breakage of drop d [−]
ϕ	dispersed phase volume fraction [−]
ρ_c	continuous phase density [$kg\,m^{-3}$]

duced and dissipated in the impeller region. They also provide large interfacial area of contact, effective radial mixing and narrow residence time distribution [3,5,6]. In addition, the mass transfer efficiency can be easily adjusted according to the requirements of the reaction. For example, using mixers that provide high energy dissipation allow the formation of small drop diameters which favors the processes with high reaction rates since they require large interfacial area of contact between the phases. Similar results can also be achieved by operating under high flow velocities. On the other hand, if the reaction is slow; lower interfacial areas and flow velocities would be sufficient. Likewise, inter-mixer spacing play also an important role in determining the extent of the reactions since they allow the control of the breakage and coalescence processes taking place where longer spaces favor the coalescence of the dispersion and shorter ones enhance the drop breakage.

Recently, a new type of static mixing element was introduced in which screens or grids are used to repetitively superimpose an adjustable uniformly distributed turbulence field in high velocity pipe flows. The subsequent low axial mixing in the contactor/reactor renders it possible to assume that plug flow conditions prevail. These characteristics made them particularly effective in processing multiphase systems and their ability to promote contact between immiscible liquids was found to be about 5-fold more energy efficient than mechanically agitated tanks equipped with Rushton-type impellers [7]. The very high turbulence intensities generated in the regions adjacent to the screens result not only in the formation of fine dispersed phase entities but also considerably enhance the value of the interphase mass transfer coefficient. The combined effect of these two factors resulted in inter-phase mass transfer coefficients as high as $13\,s^{-1}$ being achieved in the case of liquid–liquid dispersions [8], and allow for 99% of equilibrium conditions to be achieved in less than 1 s. Furthermore, such high performance allowed for orders of magnitude reduction in the reactor volume when applied to desulfurization processes [9].

Such performance improvements of multiphase contactors/reactors were attained by phenomenological interpretations of the role that turbulence has on multiphase contacting. Further optimization of their performance would thus be improved by the use of mathematical models that can accurately predict the temporal evolution of drop sizes distributions. This necessitates the use of population balance equations (PBEs) to handle drop breakage and coalescence within various regions of the contactor, and the identification of the breakage/coalescence kernels that can accurately describe these processes.

The widespread use of PBE as a tool to describe dispersed phase operations emerged from its capability to describe drop breakage and coalescence processes in terms of identifiable physical parameters and operational conditions. However, the ultimate success of this approach relies on the ability of PBE to yield realistic and accurate description of the overall drop breakage/coalescence processes.

The objective of this work is to explore the possibility of using PBE to accurately simulate drop breakage and coalescence processes in turbulently flowing liquid–liquid dispersions taking place in multi-stage screen-type static mixers (where alternating breakage-dominated and coalescence dominated regions exist).

Furthermore, since the hydrodynamic conditions prevailing in screen-type static mixers closely approach those of isotropic homogeneous turbulence, the drop breakage/coalescence kernels identified in this investigation are expected to apply to other more complex hydrodynamic conditions (such as those encountered in mechanically agitated tanks [MAT]) provided that the contactor/reactor volume is subdivided into a large number of segments where isotropic homogeneous turbulence can be correctly assumed to prevail.

2. Drop breakage and coalescence in turbulently flowing liquid–liquid dispersions

Information concerning the temporal variation of the dispersed phase characteristics (e.g. size, mass, temperature, age, and species concentration) can be obtained using the population balance equations, where the dispersed phase is considered as an assembly of drops whose individual identities are being continually destroyed and recreated by the dynamic processes occurring within the system. Under such conditions, the change in the interfacial area of contact between the phases is mainly affected by the hydrodynamics and the interfacial forces. In a two-phase turbulent flow, breakage and coalescence processes take place simultaneously until a quasi-equilibrium state is reached, where the dispersion and

coalescence rates become comparable and no net changes in drop size and drop size distribution are observed.

Even though most of the breakage and coalescence models were developed using sound thermo-, and hydro-dynamical theories, most of their validation was conducted using data obtained in mechanically agitated tanks where the complex hydrodynamics encountered in such units were often over-simplified by assuming perfectly mixed conditions with uniform energy dissipation rates. This deficiency was recently mitigated by sub-dividing the contactor volume into 2–24 compartments [10–14] where, different, but uniform value of the turbulent energy dissipation rate is assumed to exist in each compartment. The errors introduced from such a discretization approach are practically eliminated when CFD is used where the contactor volume is divided into a very large number of sub-regions. Unfortunately, most CFD tests used to test pertinent population balance (PB) kernels suffer from the uncertainties associated with the use of incomplete inter-phase momentum closures, and turbulence modulation relations, needed to accurately describe the interaction between the phases in the Eulerian–Eulerian approach [15].

In addition, the discrimination between the many expressions used to describe the sub-processes involved in the breakage and coalescence models cannot be properly undertaken because of the lack of experimental results obtained under well-known and controlled hydrodynamic conditions[16,17].

Conversely, most of the aforementioned hydrodynamic modeling difficulties are eliminated under the flow conditions encountered in multi-stage screen-type static mixers developed by Al Taweel and Chen [7]. The residence time distributions are very narrow (essentially plug flow) and the characteristics of the turbulence generated in the region downstream from each consecutive screen are well known. These mixers therefore offer a good alternative to conventional MAT mixers for developing and testing the various hydrodynamic models as they overcome the difficulties associated with the high spatial variations of the energy dissipation rates as well as flow recirculation non-uniformities. In addition, the nearly plug flow conditions present in the multi-stage screen-type contactor allow for the direct integration of the non-linear integro-differential equations obtained by applying the PBE, thereby eliminating any computational uncertainties and errors introduced through the use of CFD.

In the following sections, the hydrodynamic conditions prevalent in screen type static mixers are discussed with an emphasis on the models used for simulating drop breakage and coalescence in turbulent flows.

2.1. Modeling energy dissipation rates in screen type static mixers

The rate of energy dissipation within the static mixer plays a crucial role in determining the drop size distribution of the emerging dispersion. The volume-average energy dissipation rate in the mixer can be calculated from the pressure drop using the following expression,

$$\varepsilon = \frac{U\Delta P}{\rho_c L_M} \tag{1}$$

However, it is well known that the local value of ε downstream from screens undergoes dramatic variation along the axis of flow with the maximum value being encountered in the immediate vicinity of the screen [18,19]. Screens can be characterized by their mesh size (M); bar size (b) (or wire diameter); and the fractional open area (α). Where, the turbulence structure generated downstream of the screen is controlled by the upstream superficial velocity as well as by those parameters. A relatively large body of knowledge is available concerning the nature of grid-generated turbulence and how it is affected by the nature of flow as well as the wire mesh used [18–22]. However, the most distinctive characteristic of flow through screens is the generation of nearly isotropic turbulence in the downstream flow. Further, the decay of grid-generated turbulence is described by power laws such as:

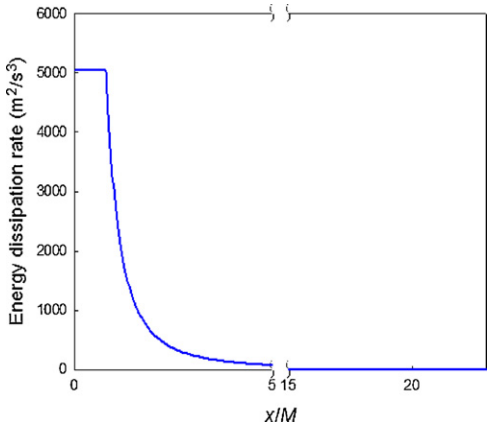

Fig. 1. Rate of energy dissipation as a function of location downstream of a screen ($U = 1.0\ \mathrm{m\,s^{-1}}$, $M = 362\ \mu\mathrm{m}$, $\alpha = 0.33$, $C = 1.81$, $n = 1.32$, $(x/M)_o = 0$, decay starts at $x = 0.8M$).

$$\left(\frac{u'}{U}\right)^2 = \frac{1}{C}\left[\frac{x}{M} - \left(\frac{x}{M}\right)_o\right]^{-n} \tag{2}$$

where C is the decay coefficient, $(x/M)_o$ is the virtual origin of turbulence decay, and n is the decay exponent.

The hydrodynamic factors affecting the performance of screen type static mixers were recently analyzed by Azizi and Al Taweel [23] who proposed that the turbulence decay profile behind a grid be divided into two regions, a region of constant high energy dissipation rate prevalent over a certain distance downstream of the grid, and a region of fast decay where the homogenous isotropic turbulence decay equation applies. Using this representation for modeling the spatial variation of the energy dissipation rate (Fig. 1), all energy sources for the flow through screens were accounted for and the calculated values matched the experimentally determined volume average ε data quite well.

The introduction of screens into the pipe flow will therefore create regions with very high energy dissipation the thickness of which depends on the screen characteristics (mesh size). However, the value of ε to which the fluid is exposed to is dramatically reduced as it flows further downstream from the screen (with up to 160-fold variation in ε being observed within a $7M$ distance downstream of the screen). The residence time within the region of high energy dissipation, and the maximum level of local energy dissipation rates encountered in these regions, are therefore a function of the screen characteristics and the superficial velocity of the fluid passing through them. Fig. 2 shows such an example, whereas very high values of local energy dissipation rates can be achieved by passing fluids through screens (up to $15{,}000\ \mathrm{W\,kg^{-1}}$ for this example of a screen with 27% open area), the corresponding residence time under such conditions is very short (as low as $420\ \mu\mathrm{s}$) unless multiple screens are used.

Additional information concerning the values of these various parameters and the proposed approach for predicting the spatial variation of the energy dissipation rate downstream of a screen are reported elsewhere [23].

2.2. Modeling of breakage and coalescence in screen-type static mixers

A variety of processes taking place in turbulently flowing dispersions induce continuous changes in the internal properties of the

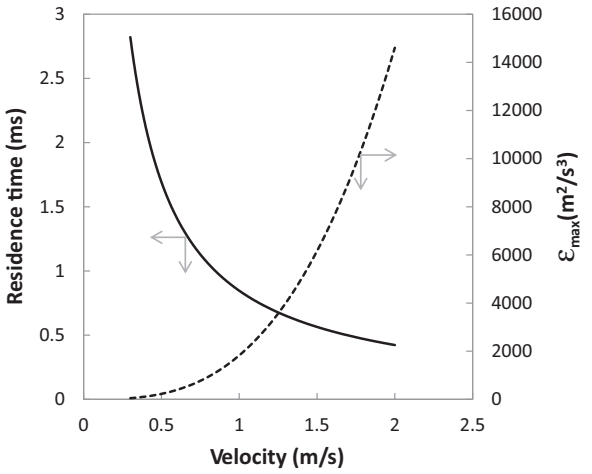

Fig. 2. Effect of superficial velocity on the maximum energy dissipation rate and the residence time in the high energy dissipation regions (M = 1058 μm, α = 0.27).

dispersed phase droplets (e.g. size, concentration and age) which consequently lose their identities. For the case of a flowing dispersion exposed to regions of high and low energy dissipation rates, the drops undergo breakage in the regions of high turbulence intensity whereas they coalesce into coarser drops while circulating in low shear regions.

Generally, drop breakage results from the interaction of a single droplet and the turbulent continuous phase eddies; therefore, if the energy gained is enough to compensate for the surface energy increase due to the expansion of the droplet surface area, then break-up occurs. Further, coalescence occurs when two drops (or more) join together into one entity. Typically, this amalgamation process consists of three successive steps. First, drops have to collide, trapping a small amount of liquid between them, the second step involves drainage of the liquid out of the film trapped between the adjacent drop surfaces, while the third and final step is the rupture of the film, after reaching a critical thickness, leading to coalescence [24]. For a flowing dispersion, as time progresses, the breakage and coalescence rates change until reaching equilibrium where the rate of both processes become virtually equal. These phenomena describing the evolution of the dispersed phase drop size distribution (DSD) can best be expressed using the population balance approach.

In its most general form the continuous PBE is a dynamic transport equation that describes the temporal evolution of population density as a result of four particulate mechanisms, namely, nucleation, growth, aggregation and breakage as well as transport due to the flow field [25]. The resulting equations are often partial integro-differential equations with integral boundary conditions that rarely admit analytical solutions, therefore the use of numerical techniques is necessary for obtaining a solution [26–28]. Consequently, the method of discretization of the continuous PBE has emerged as an attractive alternative to the various other numerical methods of solutions [29–31] and has been successfully employed, starting with the work of [32], to render accurate numerical solutions of the PBE [16,33–35].

For the case at hand, the flow within the multi-stage screen-type static mixer can be considered as radially uniform because of the flat velocity profiles induced by the screens and the relatively small spacing between consecutive elements. To accommodate the large axial variation in turbulence intensity and energy dissipation rates depicted in Fig. 1, the hydrodynamic performance of the static mixer was modeled by dividing it into very thin cells where uniform isotropic hydrodynamic conditions can be correctly assumed to exist (Fig. 3).

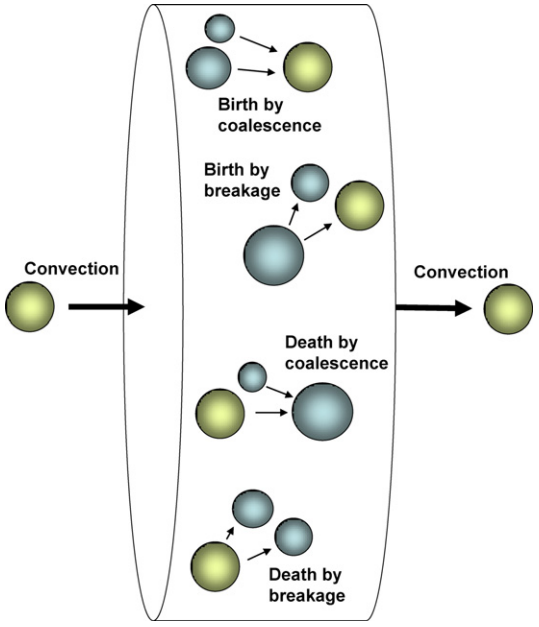

Fig. 3. Schematic representation of the PBE cell.

In the case of a well-mixed physical volume, in which there is no convection and no changes in temperature, concentration, and other internal variables are taking place, one is only concerned with dispersed phase breakage and coalescence occurrences in uniform spatial energy dissipation rate (Fig. 3).

Under such conditions, the rate of change of concentration of drops of diameter d with time can be expressed as a uni-dimensional PBE. For a locally isotropic turbulent field, this equation can be written as,

$$\left.\frac{\partial N(d,t)}{\partial t}\right|_d = B_b(d,t) - D_b(d,t) + B_c(d,t) - D_c(d,t) \tag{3}$$

where $N(d,t)$ is the number density of drop size d. B_b, D_b, B_c, and D_c are the birth rate by breakage, death rate by breakage, birth rate by coalescence, and death rate by coalescence, respectively. Further, the rates of drop birth and death by breakup can be expressed as [36]

$$B_b(d,t) = \int_d^{d_{\max}} \beta(d',d) \times \nu(d') \times g(d') \times N(d',t)\,dd' \tag{4}$$

$$D_b(d,t) = g(d) \times N(d,t) \tag{5}$$

where, $g(d')$ is the breakage frequency, $\nu(d')$ is the number of dispersed fluid entities formed from breakage of a drop of size d', and $\beta(d',d)$ is the size distribution of daughter drops formed from breakage of a drop of size d'.

In addition, the rates of drop birth and death by coalescence are written as:

$$B_c(d,t) = \int_0^{d/2^{1/3}} h\left(\left(d^3 - d'^3\right)^{1/3}, d'\right) \times \lambda\left(\left(d^3 - d'^3\right)^{1/3}, d'\right) \times N\left(\left(d^3 - d'^3\right)^{1/3}, t\right) \times N(d',t)\,dd' \tag{6}$$

$$D_c(d,t) = N(d,t) \int_0^{(d^3-d^3)^{1/3}} h(d,d') \times \lambda(d,d') \times N(d',t)\,dd' \tag{7}$$

where, $\lambda(d,d')$ is the coalescence efficiency between drops of size d and d', and $h(d,d')$ is the collision frequency between those of size d and d'.

This population balance representation is applicable to both gas–liquid and liquid–liquid dispersions provided that appropriate expressions for the various breakage and coalescence sub-processes are used. Such models have been presented by several authors, many of which have been recently reviewed by [37,38].

Coulaloglou and Tavlarides [36] developed a phenomenological model to describe drop breakage and coalescence in turbulently flowing liquid–liquid dispersions. This model assumes a locally isotropic turbulent field where both phases are moving at the same velocity. In addition, the system is considered isothermal with no interphase mass transfer or reactions are taking place, and that only turbulent fragmentation and amalgamation occur. Since all these aforementioned conditions can be held valid in this work, this model will therefore be used to describe breakage and coalescence phenomena.

In addition, this model seems to be the most widely used over the past few decades, because its ability to encompass the various physical and hydrodynamical properties of the system in the drop rate functions and provides a better physical understanding of the processes taking place. Further, this model constituted the basis from which most of the breakage and coalescence models in turbulently flowing dispersions for both gas–liquid and liquid–liquid systems were derived (e.g. Prince and Blanch [39]; Luo and Svendsen [40]).

A discussion of the various breakage and coalescence sub-processes employed in this work will thus be presented in the following sections.

2.2.1. Breakage frequency

Breakage models have been generally modeled using a combination of the collision frequency between the drops and turbulent eddies as well as the probability that a collision leads to a successful breakage. For drop sizes falling within the inertial sub-range, Coulaloglou and Tavlarides [36] assumed that the fraction of drops breaking is proportional to the fraction of drops which have a total kinetic energy greater than a minimum value necessary to overcome the surface energy holding the drop intact. Moreover, the distribution of the total kinetic energy of the drops was considered proportional to the distribution of the kinetic energies of the turbulent eddies. Based on the aforementioned considerations, Coulaloglou and Tavlarides proposed the following breakage frequency function,

$$g(d) = C_1 \times \frac{\varepsilon^{1/3}}{d^{2/3} \times (1+\phi)} \times \exp\left[-C_2 \times \frac{\sigma(1+\phi)^2}{\rho_d \times \varepsilon^{2/3} \times d^{5/3}}\right] \quad (8)$$

This function predicts a maximum frequency as the drop size increases [38,41,42]. This is inherent to the model which accounts for the time required for breakage to estimate the breakage rate. Consequently, after reaching a critical drop size, the breakage rate decreases as it becomes influenced by the breakage time [42]. Depending on the turbulence intensity and the model constants employed in this study, the maximum can reach values as low as 200 μm. However, this has minimal impact in this work, because under the current operating conditions, the breakage frequency maximum always lies outside the DSD range except for the few milliseconds (Fig. 2) where the dispersion (at the highest studied velocities) passes through the regions of very high turbulence downstream of the screens.

2.2.2. Number of daughter drops

The average number of daughter drops, $\nu(d')$, formed upon the breakage of a parent drop of diameter d', generally depends on the forces applied on the parent drop, the interfacial tension of that drop and its diameter [43]. However, this term is usually assumed to be two (i.e. binary breakage) which is considered as a valid assumption by Andersson and Andersson [44] who found that the probability of binary breakage increases with an increase in the energy dissipation rate; a condition that is expected to hold true in the current work where very high energy dissipation rates are expected to prevail in tubular reactors/contactors equipped with screen-type static mixers. This is also in accordance with the work of Maass et al. [45] who reported that binary breakage has the highest probability of occurrence for drops with sizes smaller than 1 mm in liquid–liquid systems. However, this issue remains unsettled for the case of liquid–liquid systems where contradicting conclusions can often be found in the literature. This is due to the fact that the viscosity of the dispersed phase has a large impact in determining the number of daughter drops born in a single breakage event [46,47].

Nonetheless, for the purpose of the current work, binary breakage will be assumed to take place, which according to Ruiz and Padilla [48] is not a restrictive assumption as the breakage of a parent drop in any number of daughter drops can be simulated efficiently by a rapid sequence of binary breakage events.

2.2.3. Breakage size distribution

In addition to the knowledge of the breakage frequency function and the number of drops formed after a breakage, the size distribution of these daughter drops is required for a complete description of the breakage sub-process. This daughter size distribution determines the probability at which drops of a certain size are formed as a result of a bigger drop being broken.

To describe binary breakage events, Coulaloglou and Tavlarides [36] utilized a purely statistical distribution to express the daughter size distribution, $\beta(d,d')$, by assuming that the function is normally distributed as reported by Valentas and Amundson [32] and written as,

$$\beta(d, d') = \frac{4.6}{d'^3} \times \exp\left[-4.5 \times \frac{(2d^3 - d'^3)^2}{(d'^3)^2}\right] \quad (9)$$

However, the use of a more sophisticated beta distribution function to describe the daughter density function has been proposed by Hsia and Tavlarides [43] and later adopted by several investigators [10,49,50]. This beta distribution has the advantage over the normal distribution proposed by Coulaloglou and Tavlarides [36] in that it produces a zero probability for the infinitely small daughter drops and the daughter drops equal to the size of the mother drop [49]. This beta function is expressed as,

$$\beta(d, d') = 90 \times \frac{d^2}{d'^3} \times \left(\frac{d^3}{d'^3}\right)^2 \times \left(1 - \frac{d^3}{d'^3}\right)^2 \quad (10)$$

In contrary to other models available in the literature [40,51], this beta distribution avoids the zero probability for the evolution of equi-sized drops; which is in line with the observations of Maass et al. [45] and Andersson and Andersson [44] who reported that the probability of equi-sized breakage is highest for liquid–liquid systems.

Furthermore, the use of the normal distribution for describing breakage processes was found to introduce erroneous behavior under high shear rates, e.g. $\varepsilon \geq 1000\,\mathrm{W\,kg^{-1}}$, and the problem was eliminated using the beta distribution function of Hsia and Tavlarides [28,43]. Since energy dissipation rates of the same order of magnitude or even higher are expected to prevail in tubular contactors/reactors equipped with screen-type static mixers, the beta distribution will therefore be adopted hereafter while describing the breakage processes.

2.2.4. Collision frequency

The collision between drops can be initiated by several different mechanisms. These include buoyancy-driven (that is collisions due to the difference in rise velocities of drops of different size), and collisions due to laminar shear occurring when drops follow the continuous fluid streamlines [39], in addition to drop coalescence resulting from turbulent interactions between the continuous and dispersed phase. However, only the latter coalescence mechanism will be considered in this investigation because the relative importance of the various mechanisms as compared to turbulence-induced collisions can be neglected under the highly turbulent conditions present in screen-type static mixers.

Coulaloglou and Tavlarides [36] derived a turbulent collision frequency model (assuming binary collisions) for drops with immobile interfaces by postulating that the mechanism of collision is analogous to collisions between molecules as described in the kinetic theory of gases. The collision frequency of drops of diameter d and d' can thus be written as,

$$h(d,d') = C_3 \times (d+d')^2 \times \left(d^{2/3} + d'^{2/3}\right)^{1/2} \times \frac{\varepsilon^{1/3}}{(1+\phi)} \quad (11)$$

The expression given in Eq. (11) is slightly different from the originally published one as it incorporates a small algebraic error identified by Hsia and Tavlarides [43].

2.2.5. Coalescence efficiency

Coulaloglou and Tavlarides [36] also presented an expression for the coalescence efficiency term which is based on the film drainage between colliding dispersed phase entities which is applicable to the case of deforming entities with immobile interfaces. It assumes that turbulence causes the two entities to collide and holds them together for a definite time while the intervening film thins under a constant force applied by turbulence. Coalescence will therefore only occur when the contact time of the bubbles is longer than the time required for draining the film entrapped in between them until it reaches its critical thickness. Therefore, the coalescence efficiency was expressed as,

$$\lambda(d,d') = \exp\left[-C_4 \times \frac{\mu_c \times \rho_c \times \varepsilon}{\sigma^2 \times (1+\phi)^3} \times \left(\frac{d \times d'}{d+d'}\right)^4\right] \quad (12)$$

In the current work, the initial film thickness and the critical thickness for film rupture are assumed to be constant and lumped into the value of the parameter C_4.

3. Results and discussion

3.1. Numerical solution of PBE

An accurate, stable, and robust algorithm for solving the discretized PBE, where uniform energy dissipation conditions inside the control volume can be correctly assumed, was recently developed by Azizi and Al Taweel [28]. This algorithm is based on minimizing the finite domain errors that often arise while discretizing the drop size domain and includes an enhanced solution stability algorithm which relies on monitoring the onset of errors in the various birth and death terms encountered in PBE. It consequently allows for corrective action to be undertaken before the errors propagate in an uncontrollable fashion, and was found to improve the stability and robustness of the solution method even under very high shear rate conditions.

This algorithm [28] also accounts for flow through systems with spatial variation of local energy dissipation rate and thus will be used in the current work to model turbulent drop breakup and coalescence in static mixers. It uses the size distribution sampling approach proposed by Sovova and Prochazka [52] and combines it with cubic spline interpolation if information in between sampling points is needed. It also employs a moving grid technique where insignificantly large drops are cut off from the drop size domain while occasionally re-adjusting the distribution to ensure volume conservation. At any particular time, the value of the birth and death terms is determined by integrating over the size domain (using Simpson's rule) and the resulting ODE is numerically solved using the adaptive step-size control for Runge-Kutta (5th order Runge-Kutta).

This algorithm was developed with the ability of using general forms of the breakage and coalescence kernels and can therefore be used to describe both liquid–liquid and gas–liquid dispersions. Further, it has the ability to predict the transient drop size distribution and the temporal variation of the various dispersed phase characteristic sizes.

In the current work, 60 sampling points were used to describe the drop size domain at every time step. For further information on the method of solution, its stability and robustness, the reader is referred to Azizi and Al Taweel [28].

Table 1
Characteristics of the woven screens investigated.

No.	Wire size, b (mm)	Mesh size, M (mm)	Open area, α (%)
I	0.508	1.058	27
II	0.152	0.362	33
III	0.305	0.845	41

3.2. Experimental determination of liquid–liquid contacting in screen-type static mixers

The operational characteristics of screen-type static mixers were investigated by El-Ali [53] using dilute liquid–liquid dispersions flowing in a 25.4 mm ID pipe. The setup shown in Fig. 4, consisted of a vertical mixing section that incorporated a set of static mixing elements whose characteristics are given in Table 1. The drop size distribution obtained at different design and operating conditions was recorded using a video camera with very short exposure times (2 μs). An adjustable intensity light source was used to provide the high intensity illumination necessary for imaging the dispersion at the very short exposure times necessary to freeze the images of the moving drops. The resulting images were analyzed using semi-automated image analysis software for measuring the sizes of the drops present in the dispersion. The resulting dispersions were characterized using various mean diameters (d_{10}, d_{20}, d_{30}, d_{32} and d_{43}), the number-, and volume-density distributions, as well as the variance around the Sauter mean diameter, d_{32}.

The system investigated was a dispersion of Bayol Oil in tap water, the physical properties of which are listed in Table 2.

A small quantity of salt (500 ppm) was added to the water in order to compensate for the uncontrolled variation in the composition of the tap water. Table 3 summarizes the range of experimental conditions investigated in this study.

Table 2
Physical properties of the phases at 25 °C.

Phase	Density, ρ ($kg\,m^{-3}$)	Viscosity, μ ($kg\,m^{-1}\,s^{-1}$)	Interfacial tension, σ ($mN\,m^{-1}$)
Water	997	1.0×10^{-3}	–
Bayol oil	792	2.26×10^{-3}	19

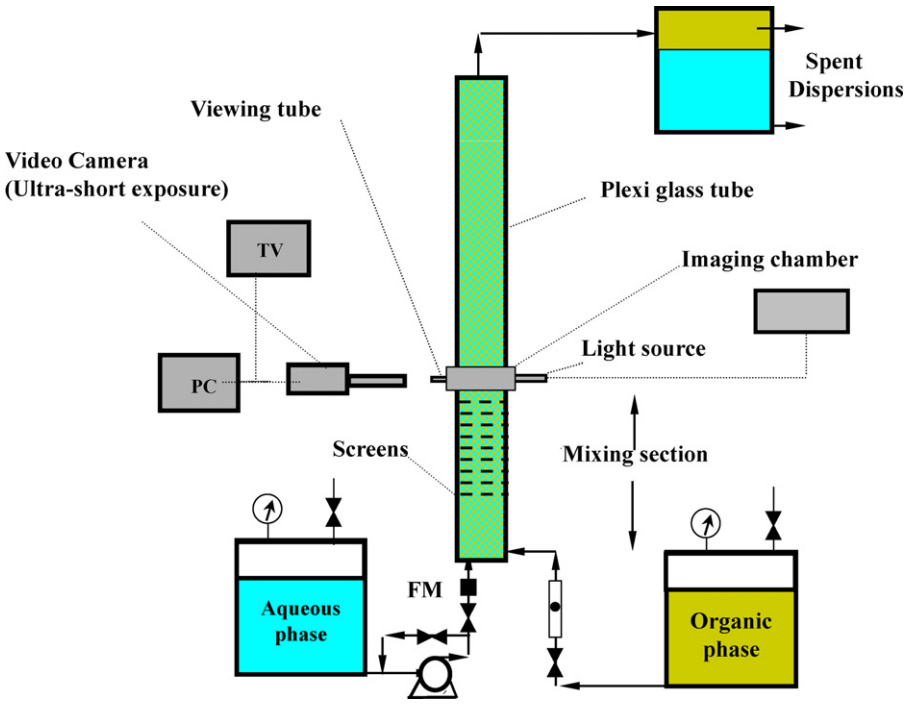

Fig. 4. Schematic representation of the experimental setup.

3.3. Comparison with experimental results

3.3.1. Determining the model constants

The experimental data represent a good case for validating the current work since it provides a large set of experimental results obtained under a wide range of design and operating conditions. Contrary to data obtained in MAT where highly non-uniform hydrodynamic conditions are encountered, these results were obtained under radially uniform turbulence conditions. The fact that turbulence in a thin slice behind screens closely approximates homogeneous isotropic conditions can be used to predict the evolution of DSD as the liquid–liquid dispersion flows through the static mixer.

In order to simulate the behavior of turbulently flowing dispersions using the Coulaloglou and Tavlarides [36] model the empirical constants used in the drop breakage/coalescence rate functions (Eqs. (8), (11) and (12)) need to be first identified. To accomplish this, the simulated quasi-steady state Sauter mean diameters were fitted against the experimentally measured ones for screen I only. The objective was to find the set of constants $(C_1 - C_4)$ that renders a global minimum for the function defined as $\sum(d_{32,\mathrm{exp}} - d_{32,\mathrm{sim}})^2$. Due to the non-linearity of the problem, this was accomplished using a Levenberg–Marquardt algorithm. Additionally, screen I was selected as representative of the various screen geometries because its hydrodynamic conditions can be considered as typical for those experimentally investigated and the values of the model constants derived thereof should be independent of the operating conditions and/or the design parameters of the mixer.

This is clearly presented in Fig. 5 which shows the variation of the quasi-equilibrium Sauter mean diameter with the superficial flow velocity after estimating the various model constants. In addition, it shows a typical drop volume density distribution using screen I. It is evident that the model predictions match the experimentally determined values with a very good accuracy, and the best fit to the experimental data was obtained using the values of the empirical constants shown in Table 4.

3.3.2. Capabilities of the simulation program

The ability of the current approach to track the variation of the drop size distribution as a function of the local energy dissipation rate along the length of the reactor can best be illustrated by following the temporal variation of the Sauter mean diameter as the immiscible dispersion flows through the static mixer (Fig. 6). As can be seen from Fig. 6, the relatively coarse drops introduced to the tubular contactor/reactor undergo a progressive reduction in the Sauter mean diameter as the dispersion passes through successive static mixing elements. A quasi-steady condition is asymptotically reached beyond which the DSD does not undergo significant changes with increasing number of mixing elements. In addition, it can be clearly discerned that the drop diameter undergoes a sharp reduction in the high energy dissipation regions adjacent to the screen before the fine bubbles formed in these regions start to coalesce as they migrate to regions of lower energy dissipation rates further downstream. This observation is similar to those reported by Turunen and Haario [5] and Andersson et al. [3] who used dif-

Table 3
Experimental conditions.

Number of screen elements	9
Inter-screen spacing	10 mm
Superficial velocity, U	0.85–1.94 ($\mathrm{m\,s^{-1}}$)
Screen open area, α	27–41%
Dispersed phase hold-up, ϕ	0.5%
Pipe Reynolds numbers	21,000–50,000

Table 4
Values of the various model constants.

Description	Symbol	Value
First breakage frequency constant	C_1	0.86 ± 0.04
Second breakage frequency constant – embedded in an exponential term	C_2	4.1 ± 0.3
Collision frequency constant	C_3	0.04 ± 0.002
Coalescence efficiency constant ($\mathrm{m^{-2}}$)	C_4	$1 \pm 0.2 \times 10^{10}$

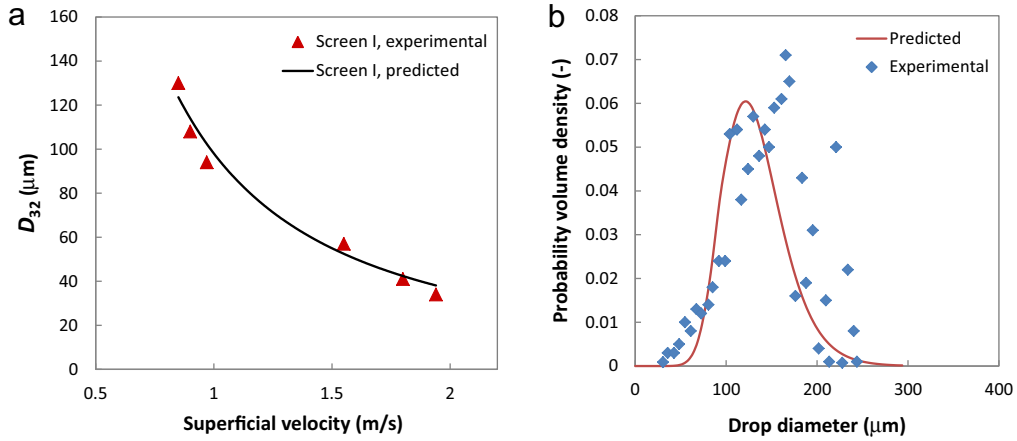

Fig. 5. (a) Variation of the Sauter mean diameter with the superficial velocity ($\alpha = 27\%$; $\phi = 0.5\%$; average deviation = ±6.52%); (b) Probability volume density distribution ($\alpha = 27\%$; $U = 0.85\ m\ s^{-1}$; $\phi = 0.5\%$).

ferent types of commercially available static mixers to promote dispersion.

The hydrodynamic conditions presented in Fig. 5a, encompass those experimentally investigated and the values of the model constants derived thereof should be independent of the operating conditions and/or the design parameters of the mixer.

Furthermore, to eliminate any effect the selection of the initial drop size distribution (DSD) might have on the solution, and to maintain consistency in the study, a normal distribution ranging from 0 to 1500 μm with a Sauter mean diameter of 750 μm was selected as the initial condition in all the simulation runs. However, the final DSD is dictated by the equilibrium between breakage and coalescence rates and thus independent of the initial DSD. Therefore, a sensitivity analysis was carried out using distributions with Sauter mean diameters varying between 500 and 1000 μm, and was found that the effect of the initial DSD dissipates after the seventh screen with average deviations up to ±11% at steady state (after the ninth screen) depending on the conditions.

In addition, the ability of the simulation program to account for the variations in the operating or design conditions is clearly evident in Fig. 7 where the quasi-steady state DSD are plotted against

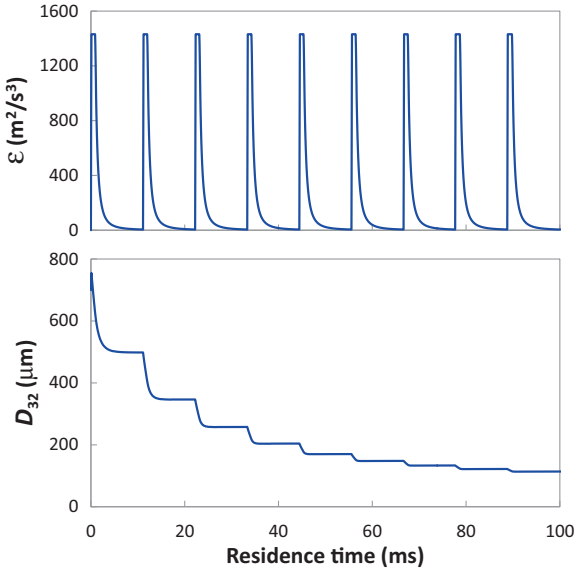

Fig. 6. Predicted spatial variation of the local energy dissipation rate and the Sauter mean diameter along the length of the contactor/reactor ($U = 0.9\ m\ s^{-1}$; $\phi = 0.5\%$; $\alpha = 0.27$).

the initial distribution. The case where the operating conditions were kept unchanged while varying the screen geometry is plotted in Fig. 7a, while that highlighting the effect of the superficial velocity on the quasi-equilibrium DSD is given in Fig. 7b for a type I screen. It is evident that the changes in the hydrodynamics of the system are well accounted for while retaining a very good resolution of the predicted DSD. This elucidates the importance of the moving grid technique used in the current work and its ability to keep the finite domain errors to a minimum by cutting insignificantly large drops from the size domain, and focus the computational efforts in the regions of most significance.

3.3.3. *Matching model predictions with experimental data*

The model constants derived in the previous section and listed in Table 4 should be a function of the physical properties of the system but independent of the operating conditions and/or the design parameters of the mixer. Therefore, these values are considered universal and will be kept unchanged throughout this investigation. However, the value of these constants were found to be several orders of magnitude larger than those obtained by previous authors who used the same model to simulate liquid–liquid dispersions using MATs [50,54–57]. The discrepancy depicted in Table 5 is most probably due to the simplifying assumptions used by these authors in which they assumed a uniform local energy dissipation rate throughout the entire volume of the MAT.

Furthermore, to highlight the difference between the various sets of constants, the cumulative number densities estimated using both the old and the new sets of model parameters were plotted against the experimentally determined values in Fig. 8. Since the older sets are of a similar magnitude, those obtained by Ribeiro et al. [57] were chosen for the purpose of this comparison. The large discrepancy between the two simulation results is clearly shown in Fig. 8 where the constants obtained in the current study predict the experimental results very well while the old constants failed to fall within the same order of magnitude as the mean diameter. This higher accuracy of the current set of constants

Table 5
Numerical values of the empirical constants in the drop rate functions.

Proposed by	C_1	C_2	C_3	$C_4\ (m^{-2})$
Coulaloglou [54]	0.00487	0.0552	2.17×10^{-4}	2.28×10^{13}
Ross et al. [55]	0.00487	0.08	2.17×10^{-4}	3×10^{12}
Hsia [56]	0.01031	0.06354	4.5×10^{-4}	1.891×10^{13}
Bapat and Tavlarides [50]	0.00487	0.08	1.9×10^{-3}	2×10^{12}
Ribeiro et al. [57]	0.00481	0.0558	1.65×10^{-3}	4.74×10^{12}
Current work	0.86	4.1	0.04	1×10^{10}

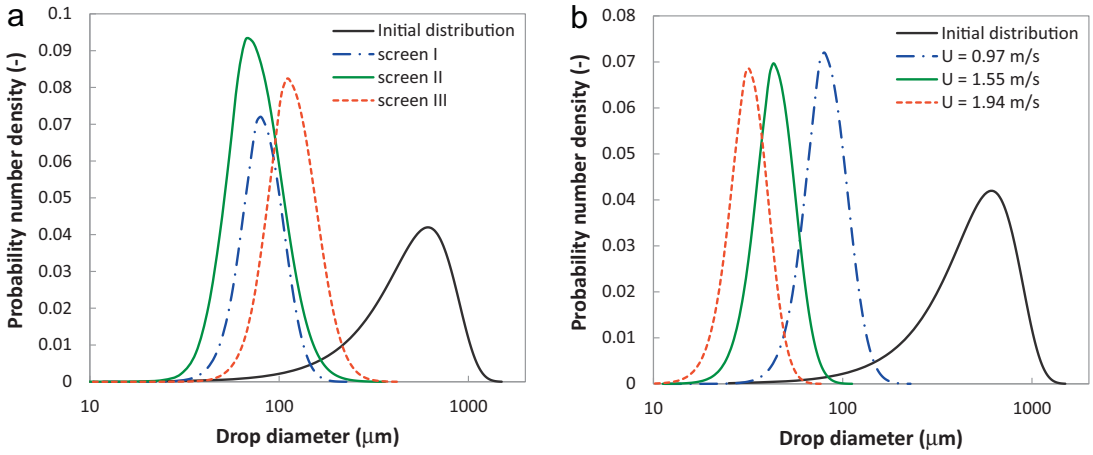

Fig. 7. Effect of varying design and operating conditions on the quasi-equilibrium DSD at $\phi = 0.5\%$. (a) Effect of screen design at $U = 0.97\ m\ s^{-1}$; (b) Effect of velocity for $\alpha = 27\%$.

emphasizes the importance of accounting for the spatial variation in the energy dissipation rates while estimating the model parameters. This unmistakably illustrates the danger of assuming simplified hydrodynamic conditions and estimating the breakage and coalescence processes under conditions that do not truly apply.

In an attempt to characterize breakage and coalescence phenomena for droplets in rotating disc contactors, Schmidt et al. [34] employed only the coalescence functions of Coulaloglou and Tavlarides [36] along with a different breakage kernel. When the model parameters were determined as independent of the hydrodynamic conditions prevailing in the system, they obtained a set of constants for the coalescence kernel that are very similar to those obtained in the current work ($C_3 = 0.036$ and $C_4 = 1.152 \times 10^{10}\ m^{-2}$). However, these results were found dependent on the chemical system used. Whereas the system exhibiting an interfacial tension comparable to the one employed in this work ($\sigma = 14\ mN\ m^{-1}$ compared to $19\ mN\ m^{-1}$ in this work) resulted in very comparable sets of constants, other chemical systems with larger interfacial tensions required the use of a different set of constants to be accurately predicted.

This however does not completely justify the order of magnitude difference in the model constants, since changes in the interfacial characteristics of the system are not expected to induce such large variations in their values. However, it is important to add that the model parameters used by Ribeiro et al. [57] for example were derived for two different systems whose interfacial tensions ranged from 9 to $32\ mN\ m^{-1}$. Therefore, even though the interfacial characteristics of the system play an important role in determining the extent of the model parameters, the importance of an accurate representation of the energy dissipation rate while characterizing breakage and coalescence processes remains imperative.

Fig. 9 clearly shows the effect of changing the operating conditions on the Sauter mean drop diameter prevalent after the ninth screen element where quasi-steady state conditions are considered to be reached. This figure shows a good match between predicted and measured Sauter mean diameters with an average deviation of ±9.51% and 6.50% for screens II and III, respectively. The average equilibrium diameter was thus found to decrease with increasing the superficial velocity while decreasing with an increase in the screen open area.

Two different drop breakage mechanisms in screen-type static mixers were identified by El-Ali [53]. While turbulent dispersion in the micro-jets prevails at high flow velocities, the droplets may undergo a physical cutting action when they impinge on the screen. The latter phenomenon, however, is more pronounced in the initial stages of dispersing large drops and at lower velocities or when very fine mesh screens are used. The relative magnitude of the measured mean diameters to the mesh openings ($0.06 < d_{32,exp}/(M - b) < 0.54$) can also be employed as an indication that turbulent breakage prevails under the investigated operating conditions.

It is well known that the superficial velocity is one of the major factors governing liquid–liquid dispersion processes as it controls the kinetic energy in the micro-jets formed by the screens, and hence the turbulent breakup and coalescence processes. In the

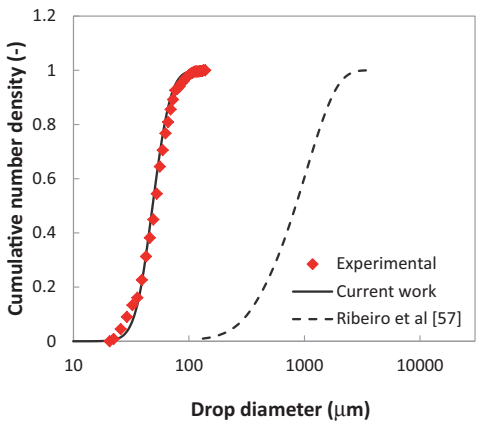

Fig. 8. Comparison between the old and new constants ($\alpha = 41\%$; $U = 1.94\ m\ s^{-1}$; $\phi = 0.5\%$).

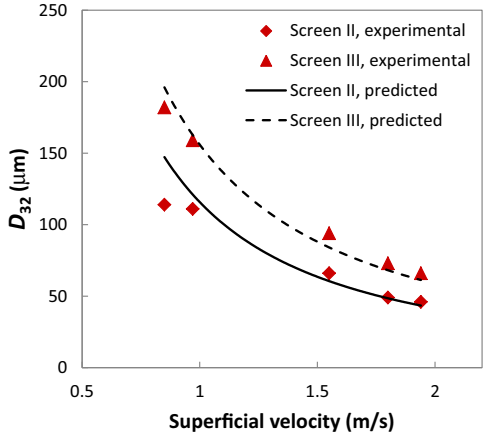

Fig. 9. Effect of screen geometry on the variation of the Sauter mean diameter with the superficial velocity ($\phi = 0.5\%$).

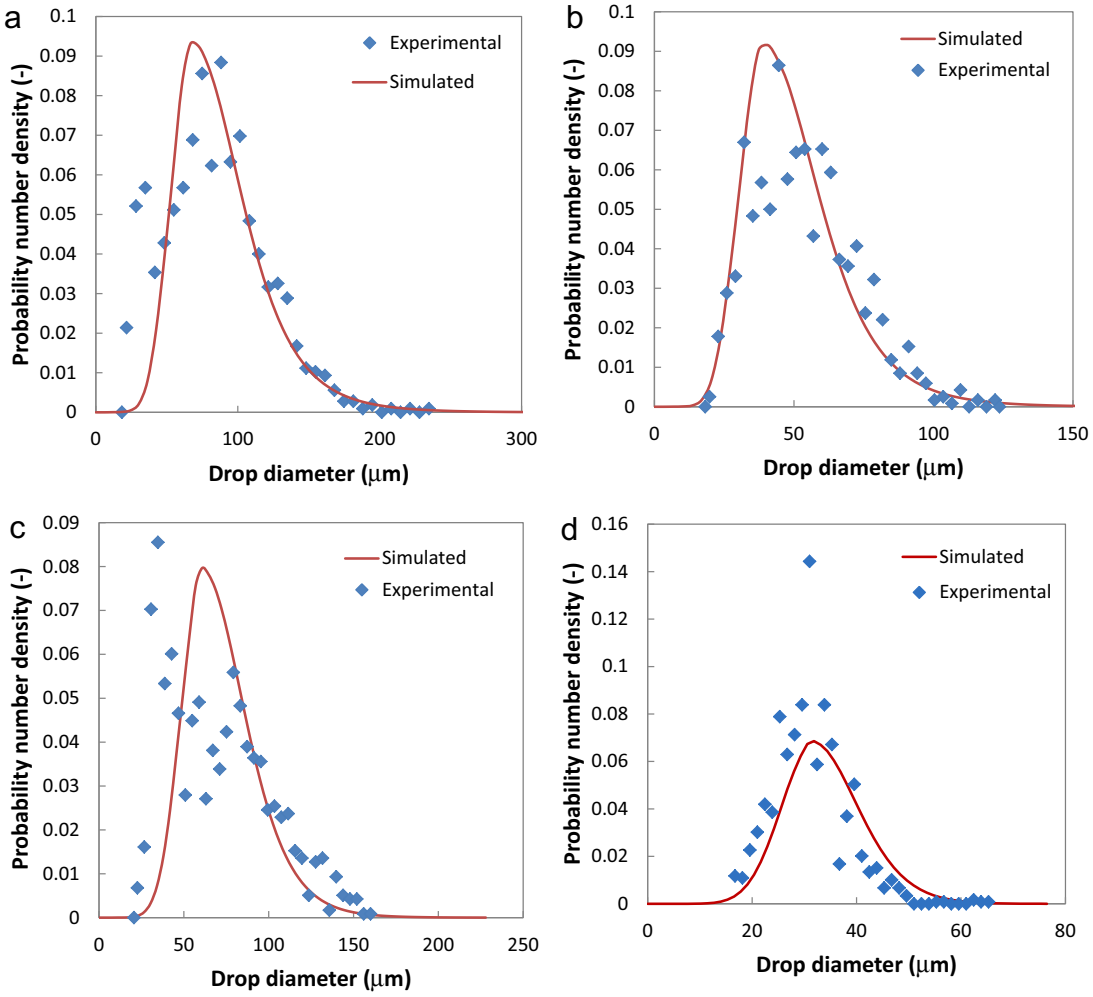

Fig. 10. Effect of varying operating and design conditions on the probability number density distributions at $\phi = 0.5\%$: (a) $\alpha = 33\%$ at $U = 0.97\ m\ s^{-1}$; (b) $\alpha = 33\%$ at $U = 1.55\ m\ s^{-1}$; (c) $\alpha = 41\%$ at $U = 1.55\ m\ s^{-1}$; (d) $\alpha = 27\%$ at $U = 1.94\ m\ s^{-1}$.

case at hand, the superficial velocity affects both the local rate of energy dissipation, ε, as well as the residence time of the fluid elements within the region of high local energy dissipation rate. Moreover, screens with lower open area are expected to produce higher velocity jets and hence higher local energy dissipation rates in the regions immediately downstream from the screens. Consequently, finer dispersions are expected as the screen open area decreases.

The fact that the model predicts the experimental observations with high accuracy is an additional indication that the hydrodynamic model responsible for predicting the spatial variation of the energy dissipation rate [23] throughout the contactor works quite well and yields good estimates of ε since good agreements between simulations and experimental data are also to a large extent based on good predictions of the turbulent energy dissipation rate [3].

The ability of the model to render accurate estimates of the DSD under a wide range of operating and design conditions is further shown in Fig. 10 where the experimental and simulation results are plotted for three different screen geometries and varying superficial velocities. Even though small deviations from the experimental values are apparent, it is clear that the simulation algorithm predicts the distributive effect with a good accuracy. While the predicted DSD fitted the experimental results accurately for screen II (Fig. 10a and b); the simulations using screens I and III deviated slightly from the measured data.

4. Conclusion

From the aforementioned findings, one can conclude that the turbulent dispersion/coalescence of liquid–liquid systems can be accurately predicted using the phenomenological model developed by Coulaloglou and Tavlarides [36]. In this study, a population balance model utilizing this kernel was developed and used to assess its ability to accurately simulate the liquid–liquid contacting performance achieved in screen-type static mixers where nearly-isotropic turbulent plug flow conditions prevail.

The predicted drop size distribution as well as the Sauter mean diameter (when quasi-steady state conditions were assumed to be reached) was compared with experimental results measured by photographic techniques and good agreement was obtained at different flow velocities and diverse screen geometries.

The successive exposure of the flowing dispersion to breakage-dominated and coalescence dominated regions provided very stringent conditions for testing and validating the model and for the development of accurate model parameters that may be used for simulating other more complex liquid–liquid contacting conditions such as those encountered in MAT.

In addition to generating very uniform hydrodynamic conditions, the major advantage of using this type of reactor is that it allows an easy optical access to each mixing element. This would be of great importance in experimentally determining breakage and

coalescence processes under well controlled and well characterized turbulent conditions.

Acknowledgment

The authors would like to acknowledge the financial support of the Natural Science and Engineering Research Council of Canada (NSERC).

References

[1] E.L. Paul, V.A. Atiemo-Obeng, S.M. Kresta, Handbook of Industrial Mixing: Science and Practice, Wiley-Interscience, Hoboken, NJ, 2004.
[2] A. Bakker, A.H. Haidari, L.M. Oshinowo, Realize greater benefits from CFD, Chem. Eng. Prog. 97 (2001) 45–53.
[3] R. Andersson, B. Andersson, F. Chopard, T. Noren, Development of a multi-scale simulation method for design of novel multiphase reactors, Chem. Eng. Sci. 59 (2004) 4911–4917.
[4] R.K. Thakur, C. Vial, K.D.P. Nigam, E.B. Nauman, G. Djelveh, Static mixers in the process industries: a review, Chem. Eng. Res. Design 81 (2003) 787–826.
[5] I. Turunen, H. Haario, Mass transfer in tubular reactors equipped with static mixers, Chem. Eng. Sci. 49 (1994) 5257–5269.
[6] A.M. Al Taweel, M. El-Ali, F. Azizi, B. Liekens, D. Odedra, A. Uppal, H.G. Gomaa, In-line processing for intensifying multi-phase contacting operations, in: Proceedings of the 5th Inter. Conf. Process Intensification, vol. 5, 2003, pp. 59–73.
[7] A.M. Al Taweel, C. Chen, Novel static mixer for the effective dispersion of immiscible liquids, Chem. Eng. Res. Design Trans. I Chem E Part A 74 (1996) 445–450.
[8] A.M. Al Taweel, C. Li, H.G. Gomaa, P. Yuet, Intensifying mass transfer between immiscible liquids: using screen-type static mixers, Chem. Eng. Res. Design 85 (2007) 760–765.
[9] A.M. Al Taweel, F. Azizi, A. Uppal, Using static mixers to intensify diesel desulfurization operations, in: Sixth International Symposium on Mixing in Industrial Process Industries – ISMIP VI, 2008.
[10] V. Alopaeus, J. Koskinen, K.I. Keskinen, Simulation of the population balances for liquid–liquid systems in a nonideal stirred tank. Part 1. Description and qualitative validation of the model, Chem. Eng. Sci. 54 (1999) 5887–5899.
[11] A.H. Alexopoulos, D. Maggioris, C. Kiparissides, CFD analysis of turbulence non-homogeneity in mixing vessels: a two-compartment model, Chem. Eng. Sci. 57 (2002) 1735–1752.
[12] M. Laakkonen, V. Alopaeus, J. Aittamaa, Validation of bubble breakage, coalescence and mass transfer models for gas–liquid dispersion in agitated vessel, Chem. Eng. Sci. 61 (2006) 218–228.
[13] S. Schmelter, Modeling, analysis, and numerical solution of stirred liquid–liquid dispersions, Comput. Methods Appl. Mech. Eng. 197 (2008) 4125–4131.
[14] G.J. Wells, W.H. Ray, Methodology for modeling detailed imperfect mixing effects in complex reactors, AIChE J. 51 (2005) 1508–1520.
[15] A.M. Al Taweel, S. Madhavan, K. Podila, M. Koksal, A. Troshko, Y.P. Gupta, CFD simulation of multiphase flow: closure recommendations for fluid–fluid systems, in: Proceedings of the 12th European Conference on Mixing, 2006, pp. 495–502.
[16] M. Laakkonen, P. Moilanen, V. Alopaeus, J. Aittamaa, Modelling local bubble size distributions in agitated vessels, Chem. Eng. Sci. 62 (2007) 721–740.
[17] C.D. Eastwood, L. Armi, J.C. Lasheras, The breakup of immiscible fluids in turbulent flows, J. Fluid Mech. 502 (2004) 309–333.
[18] J. Groth, A.V. Johansson, Turbulence reduction by screens, J. Fluid Mech. 197 (1988) 139–155.
[19] G. Briassulis, J.H. Agui, Y. Andreopoulos, The structure of weakly compressible grid-generated turbulence, J. Fluid Mech. 432 (2001) 219–283.
[20] M. Gad-el-hak, S. Corrsin, Measurements of the nearly isotropic turbulence behind a uniform jet grid, J. Fluid Mech. 62 (1974) 115–143.
[21] M. Lance, J. Bataille, Turbulence in the liquid phase of a uniform bubbly air–water flow, J. Fluid Mech. 222 (1991) 95–118.
[22] H.S. Kang, S. Chester, C. Meneveau, Decaying turbulence in an active-grid-generated flow and comparisons with large-eddy simulation, J. Fluid Mech. (2003) 129–160.
[23] F. Azizi, A.M. Al Taweel, Hydrodynamics of flow through screens and screen-type static mixers, Chem. Eng. Comm. 198 (2011) 1–17.
[24] B.C.H. Venneker, J.J. Derksen, H.E.A. Van den Akker, Population balance modeling of aerated stirred vessels based on CFD, AIChE J. 48 (2002) 673–685.
[25] S. Rigopoulos, A.G. Jones, Finite-element scheme for solution of the dynamic population balance equation, AIChE J. 49 (2003) 1127–1139.
[26] A.W. Mahoney, D. Ramkrishna, Efficient solution of population balance equations with discontinuities by finite elements, Chem. Eng. Sci. 57 (2002) 1107–1119.
[27] M.M. Attarakih, H. Bart, N.M. Faqir, Numerical solution of the spatially distributed population balance equation describing the hydrodynamics of interacting liquid–liquid dispersions, Chem. Eng. Sci. 59 (2004) 2567–2592.
[28] F. Azizi, A.M. Al Taweel, Algorithm for the accurate numerical solution of PBE for drop breakup and coalescence under high shear rates, Chem. Eng. Sci. 65 (2010) 6112–6127.
[29] S. Kumar, D. Ramkrishna, On the solution of population balance equations by discretization. I: A fixed pivot technique, Chem. Eng. Sci. 51 (1996) 1311–1332.
[30] S. Kumar, D. Ramkrishna, On the solution of population balance equations by discretization. II: A moving pivot technique, Chem. Eng. Sci. 51 (1996) 1333–1342.
[31] N.E. Balliu, I.T. Cameron, R. Newell, A comparative study of numerical methods for solving continuous population balance models for aggregation processes, Dev. Chem. Eng. Miner. Process. 12 (2004) 277–291.
[32] K.J. Valentas, N.R. Amundson, Breakage and coalescence in dispersed phase systems, Ind. Eng. Chem. Fund. 5 (1966) 533–542.
[33] V. Alopaeus, J. Koskinen, K.I. Keskinen, J. Majander, Simulation of the population balances for liquid–liquid systems in a nonideal stirred tank. Part 2: Parameter fitting and the use of the multiblock model for dense dispersions, Chem. Eng. Sci. 57 (2002) 1815–1825.
[34] S.A. Schmidt, M. Simon, M.M. Attarakih, L. Lagar, G.H. Bart, Droplet population balance modelling: hydrodynamics and mass transfer, Chem. Eng. Sci. 61 (2006) 246–256.
[35] F. Azizi, A.M. Al Taweel, Population balance simulation of gas–liquid contacting, Chem. Eng. Sci. 62 (2007) 7436–7445.
[36] C.A. Coulaloglou, L.L. Tavlarides, Description of interaction processes in agitated liquid–liquid dispersions, Chem. Eng. Sci. 32 (1977) 1289–1297.
[37] H.A. Jakobsen, H. Lindborg, C.A. Dorao, Modeling of bubble column reactors: progress and limitations, Ind. Eng. Chem. Res. 44 (2005) 5107–5151.
[38] J.C. Lasheras, C. Eastwood, C. Martinez-Bazan, J.L. Montanes, A review of statistical models for the break-up of an immiscible fluid immersed into a fully developed turbulent flow, Int. J. Multiphase Flow 28 (2002) 247–278.
[39] M.J. Prince, H.W. Blanch, Bubble coalescence and break-up in air-sparged bubble columns, AIChE J. 36 (1990) 1485–1499.
[40] H. Luo, H.F. Svendsen, Theoretical model for drop and bubble breakup in turbulent dispersions, AIChE J. 42 (1996) 1225–1233.
[41] Y. Liao, D. Lucas, A literature review of theoretical models for drop and bubble breakup in turbulent dispersions, Chem. Eng. Sci. 64 (2009) 3389–3406.
[42] S. Maass, F. Metz, T. Rehm, M. Kraume, Prediction of drop sizes for liquid–liquid systems in stirred slim reactors. Part I: Single stage impellers, Chem. Eng. J. 162 (2010) 792–801.
[43] M.A. Hsia, L.L. Tavlarides, Simulation model for homogeneous dispersions in stirred tanks, Chem. Eng. J. Biochem. Eng. J. 20 (1980) 225–236.
[44] R. Andersson, B. Andersson, On the breakup of fluid particles in turbulent flows, AIChE J. 52 (2006) 2020–2030.
[45] S. Maass, A. Gabler, A. Zaccone, A.R. Paschedag, M. Kraume, Experimental investigations and modelling of breakage phenomena in stirred liquid/liquid systems, Chem. Eng. Res. Des. 85 (2007) 703–709.
[46] W. Podgorska, Daughter particle distribution for liquid–liquid dispersion in a turbulent flow, Inz. Chem. Procesowa 27 (2006) 431–441.
[47] S. Tcholakova, N. Vankova, N.D. Denkov, T. Danner, Emulsification in turbulent flow. 3: Daughter drop-size distribution, J. Colloid Interface Sci. 310 (2007) 570–589.
[48] M.C. Ruiz, R. Padilla, Analysis of breakage functions for liquid–liquid dispersions, Hydrometallurgy 72 (2004) 245–258.
[49] P.M. Bapat, L.L. Tavlarides, Mass transfer in a continuous flow stirred tank reactor, in: International Solvent Extraction Conference, ISEC '83, 1983, pp. 108–109.
[50] P.M. Bapat, L.L. Tavlarides, Mass transfer in a liquid–liquid CFSTR, AIChE J. 31 (1985) 659–666.
[51] C. Tsouris, L.L. Tavlarides, Breakage and coalescence models for drops in turbulent dispersions, AIChE J. 40 (1994) 395–406.
[52] H. Sovova, J. Prochazka, Breakage, Coalescence of drops in a batch stirred vessel. 1: Comparison of continuous and discrete models, Chem. Eng. Sci. 36 (1981) 163–171.
[53] M. El-Ali, Performance characteristics of a novel liquid–liquid contactor, PhD Thesis, Dalhousie University, Canada, 2001.
[54] C.A. Coulaloglou, Dispersed phase interactions in an agitated flow vessel, PhD Thesis, Illinois Institute of Technology, Chicago, IL, USA, 1975.
[55] S.L. Ross, F.H. Verhoff, R.L. Curl, Droplet breakage and coalescence processes in an agitated dispersion. 2: Measurement and interpretation of mixing experiments, Ind. Eng. Chem. Fund. 17 (1978) 101–108.
[56] M.A. Hsia, The modeling of liquid–liquid extraction in stirred tanks by a simulation approach, PhD Thesis, Illinois Institute of Technology, Chicago, IL, USA, 1981.
[57] L.M. Ribeiro, P.F.R. Regueiras, M.M.L. Guimaraes, C.M.N. Madureira, J.J.C. Cruz-Pinto, Dynamic behaviour of liquid–liquid agitated dispersions. I: The hydrodynamics, Comput. Chem. Eng. 19 (1995) 333–343.